Carbohydrate Polymers 137 (2016) 726–731

Contents lists available at ScienceDirect

Carbohydrate Polymers

journal homepage: www.elsevier.com/locate/carbpol

Facile synthesis of cobalt ferrite nanotubes using bacterial nanocellulose as template

S. Menchaca-Nal[a], C.L. Londoño-Calderón[a], P. Cerrutti[b], M.L. Foresti[a], L. Pampillo[c], V. Bilovol[c], R. Candal[d], R. Martínez-García[e,*]

[a] Institute of Polymer Technology and Nanotechnology, Faculty of Engineering, University of Buenos Aires—CONICET, Argentina
[b] Department of Chemical Engineering, Faculty of Engineering, University of Buenos Aires, Argentina
[c] Institute of Technology and Engineering Sciences "Hilario Fernández Long", Faculty of Engineering, University of Buenos Aires—CONICET, Argentina
[d] Institute of Physical Chemistry of Materials Environment and Energy, Faculty of Natural Sciences, University of Buenos Aires—CONICET, Argentina
[e] Faculty of Natural Resources, National University of Formosa—CONICET, Campus Universitario, Modulo I, Av. Gutnisky 3200, Formosa, Argentina

ARTICLE INFO

Article history:
Received 8 July 2015
Received in revised form 16 October 2015
Accepted 18 October 2015
Available online 20 October 2015

Keywords:
Bacterial nanocellulose
Cobalt ferrite
Nanotubes
Biotemplate

ABSTRACT

A facile method for the preparation of cobalt ferrite nanotubes by use of bacterial cellulose nanoribbons as a template is described. The proposed method relays on a simple coprecipitation operation, which is a technique extensively used for the synthesis of nanoparticles (either isolated or as aggregates) but not for the synthesis of nanotubes. The precursors employed in the synthesis are chlorides, and the procedure is carried out at low temperature (90 °C). By the method proposed a homogeneous distribution of cobalt ferrite nanotubes with an average diameter of 217 nm in the bacterial nanocellulose (BC) aerogel (3%) was obtained. The obtained nanotubes are formed by 26–102 nm cobalt ferrite clusters of cobalt ferrite nanoparticles with diameters in the 9–13 nm interval. The nanoparticles that form the nanotubes showed to have a certain crystalline disorder, which could be attributed in a greater extent to the small crystallite size, and, in a lesser extent, to microstrains existing in the crystalline lattice. The BC-templated-$CoFe_2O_4$ nanotubes exhibited magnetic behavior at room temperature. The magnetic properties showed to be influenced by a fraction of nanoparticles in superparamagnetic state.

© 2015 Elsevier Ltd. All rights reserved.

1. Introduction

Due to their promising applications in diverse fields of scientific development, different inorganic nanoparticles/biopolymers nanocomposite materials have recently been the focus of much interest from the academic and industrial community (Chen, Yang, Ma, & Wu, 2011; Hassan-Nejad, Ganster, Bohn, Pinnow, & Volkert, 2009; Kroll & Winnik, 1996; Llanes, Ryan, & Marchessault, 2000). For this kind of nanocomposites the most promising applications involve biomedicine uses (Chen et al., 2011), heavy metal separation (Fatyasari, Sureshkumar, & Lee, 2011; Zhoua, Branford-White, Nie, & Zhua, 2009), electronic devices (Aoki, Huang, & Kunitake, 2006) and photovoltaics (Zheng et al., 2013).

The combination of inorganic nanoparticles and cellulose takes benefit from the properties of both components, resulting in new properties due to synergistic effects (Hu, Chen, Yang, Li, & Wang, 2014; Klemm et al., 2006). In this context, nanocellulose is an ideal template to prepare several nanostructures (Hu et al., 2014; Li et al., 2012; Olsson et al., 2010). Recently, nanocellulosics have been successfully used as template for the growth of isolated metal nanoparticles and metal nanotubes (Gu, Liu, Niu, & Huang, 2010; Li et al., 2012; Olsson et al., 2010). Among nanocellulose sources, bacterial nanocellulose is biosynthesized as primary extracellular metabolite by certain bacteria which under proper conditions secrete high-quality cellulose ribbons of microfibrillar bundles. Micrometric-in-length BC ribbons typically show rectangular cross-sections with thicknesses around 3–4 nm and widths in the 70–100 nm interval (Bielecki, Krystynowicz, Turkiewicz, & Kalinowska, 2002). The biopolymer is obtained as a highly hydrated pellicle (97–99%) in the air–water interface of static fermentation vials, and it is recognized for its unique physicochemical, biological and mechanical properties such as high water holding capacity, high crystallinity, high tensile strength and Young modulus, biodegradability, biocompatibility and low thermal expansion coefficient in the axial direction, among others (Castro et al., 2011; Klemm et al., 2011; Putra, Kakugo, Furukawa, Gong, & Osada, 2008). Based on its outstanding properties, BC has a wide range of potential technical applications (Charreau, Foresti, & Vázquez, 2013; Klemm et al., 2011).

* Corresponding author. Tel.: +5411-4342-1396; fax: +5411-4342-1396.
E-mail address: rmartinez@fi.uba.ar (R. Martínez-García).

http://dx.doi.org/10.1016/j.carbpol.2015.10.068
0144-8617/© 2015 Elsevier Ltd. All rights reserved.

Cobalt ferrite ($CoFe_2O_4$) nanoparticles attract interest due to their magnetic properties and their high mechanical and chemical stability (Dorsey, Lubitz, Chrisey, & Horwitz, 1996). Cobalt ferrite is a ferrimagnet with a cubic spinel structure. The Fe^{3+} and Co^{2+}/Fe^{3+} ions occupy the tetrahedral (A sites) and octahedral (B sites), respectively, with a formal ionic distribution that can be represented by $(Fe^{3+})_A(Fe^{3+}Co^{2+})_BO_4^{2-}$ (Valenzuela, 1994). $CoFe_2O_4$ nanotubes have been obtained by electrospinning (Fu et al., 2012), as well as by atomic layer deposition (ALD) onto cellulose (Korhonen et al., 2011) and using anodic alumina oxide (Hua et al., 2007) templates. On the other hand, BC/cobalt ferrite nanocomposites have also been prepared by coprecipitation; however, by this comparatively cheaper and simpler methodology have led to isolated nanoparticles embedded within the nanocellulosics substrate, and not to the formation of nanotubes (Olsson et al., 2010; Zhang et al., 2011).

In the current contribution, a facile procedure for the synthesis of $CoFe_2O_4$ nanotubes is proposed. The method relies on the *in situ* precipitation of metal ions onto freeze-dried bacterial cellulose nanoribbons (nucleation sites). Cobalt chloride and iron chloride salts are used as precursors, being the iron cation in the 3+ state, which differs from previously reported methodologies (Olsson et al., 2010). Moreover, by use of Iron (III) chloride no extra oxidation step for $CoFe_2O_4$ formation is required. The described method leads to homogeneous cobalt ferrite biotemplated-nanotubes. $CoFe_2O_4$ nanotubes obtained by the simple non-expensive methodology herein proposed were characterized by means of scanning electron microscopy (SEM), X-ray diffraction (XRD), Mössbauer spectroscopy, thermogravimetric analysis (TGA) and magnetometry.

2. Experimental

2.1. Microorganism and culture conditions

Inocula were cultured at 28 °C for 48 h in 100 mL Erlenmeyers flasks containing 20 mL of Hestrin and Schramm (HS) medium (%, w/v): anhydrous dextrose (Biopack), 2.0; meat peptone (Britania, Laboratorios Britania S.A.), 0.5; yeast extract (Britania, Laboratorios Britania S.A.), 0.5; anhydrous disodium phosphate (Anhedra), 0.27; citric acid (Merck), 0.15. The pH was adjusted to 6.0 with dilute HCl or NaOH. Agitation (200 rpm) was provided by an orbital shaker.

The fermentation media was HS broth modified by using glycerol (2% w/v) instead of dextrose. The fermentation media was inoculated with 1% v/v of the inoculum culture and distributed in 250 mL Erlenmeyer flasks, keeping the ratio "volume flask: volume medium" in 5:1. The incubation was performed in a shaking water bath (130 rpm) at 28 °C for 15 days. The cellulose pellicles obtained were separated from the culture media by filtration through two layers of cotton gauze and washed at least five times with distilled water. The product was then freeze-dried by use of Christ Alpha 1-4 LD equipment for 48 h to preserve the open porous structure of the cellulose in the dry state. Previous coprecipitation methodologies which led to isolated $CoFe_2O_4$ over BC nanoribbons used lower freeze-dried time intervals, i.e. 12 h (Olsson et al., 2010).

2.2. $CoFe_2O_4$ nanotubes synthesis

Previously freeze-dried BC pieces (20 mg) were immersed for 15 min in 200 mL of a freshly prepared solution 0.02 mol of $FeCl_3{\cdot}6H_2O$ (Anedra, Research AG S.A) and 0.01 mol of $CoCl_2{\cdot}6H_2O$ (Anedra, Research AG S.A). The system was maintained at room temperature. The molar ratio remained 2:1 [Fe]/[Co] in the precursor salts (Tourinho, Franck, & Massart, 1990). Almost immediately, BC color changed from white to orange. The solution containing the BC was then heated at 90 °C for 3 h. This process helps to promote the transformation of soluble initial metal hydroxides to insoluble metal oxyhydroxide complexes that in later stages convert into $CoFe_2O_4$ (Olsson et al., 2005). BC was subsequently transferred to a solution of 1.2 M NaOH (Laboratorios Cicarelli, Reagents S.A) and the system was kept at 90 °C for 6 h. The color of BC changed rapidly from orange to black, which indicated the formation of cobalt ferrite. The product obtained was then washed with distilled water repeatedly to remove counterions, and finally dried at room temperature for 96 h.

2.3. Characterization methods

Samples were coated with a thin layer of gold using an ion sputter coater, and their morphology and structure were analyzed with a Field Emission Scanning Electron Microscope (FE-SEM, Zeiss Supra 40) with field emission gun operated at 3 kV. The gray-scale imaging process was developed to determine the porosity of the samples by using a scanning probe image processor ImageJ-1.46r (Schneider, Rasband, & Eliceiri, 2012). The X-ray diffraction (XRD) patterns were recorded in a Rigaku diffractometer with Cu Kα radiation in a 2θ range from 10° to 100°. Thermogravimetric analysis (TGA) of previously dried (110 °C, 1 h) samples was conducted in a TGA-50 Shimadzu instrument. Temperature programs were run from 25 °C to 800 °C at a heating rate of 10 °C/min, under nitrogen atmosphere (30 mL/min) in order to prevent thermoxidative degradation. Magnetic properties were analyzed using a Physical Property Measurement System (PPMS, Quantum Design). Magnetization curves as a function of applied field were obtained at different temperatures (5 and 300 K) between −40 and 40 kOe. M_S values were expressed per gram of magnetic mass as emu/g $CoFe_2O_4$. A ^{57}Fe Mössbauer spectrum was recorded in transmission geometry at room temperature using a $^{57}Co/Rh$ α-ray source mounted on an electromagnetic transducer with a triangular velocity form. The hyperfine structure was modeled by least-squares fitting procedure of Gaussian lines. The isomer shift (IS) values were referred to α-Fe at 300 K.

3. Results and discussion

3.1. $CoFe_2O_4$ nanotubes synthesis

The nanocellulosic template used in the current contribution was freeze-dried bacterial nanocellulose. Freeze-dried BC nanoribbons have high affinity for water. When the three-dimensional BC network contacts the aqueous precursor solution, the nanoribbons are negatively charged due to the presence of hydroxyl groups moieties that are exposed to the surface of the fiber. Metal precursors (Fe^{3+} and Co^{2+} ions) thus bind to cellulose nanofibrils via electrostatic (i.e., ion-dipole) interactions between the hydroxyl groups (electron-rich oxygen atoms) of BC and the electropositive transition metal cations (Shilin, Qiufang, Dandan, Tengfei, & Xiaoya, 2012). The formed oxyhydroxides act as nucleation points for the growing of nanoparticles that form the nanotubes. The relatively low temperature (90 °C) used in the synthesis contributes to the formation of homogeneous nanotubes using BC as template. The chosen temperature leads to slow nucleation and growing of the particles that form the nanotubes and contributes to obtaining homogeneous structures. During the later drying process, the initially swollen cellulose nanoribbons are dried, leading to the formation of hollow metal oxide structures with dried cellulose nanoribbons remaining in their interior.

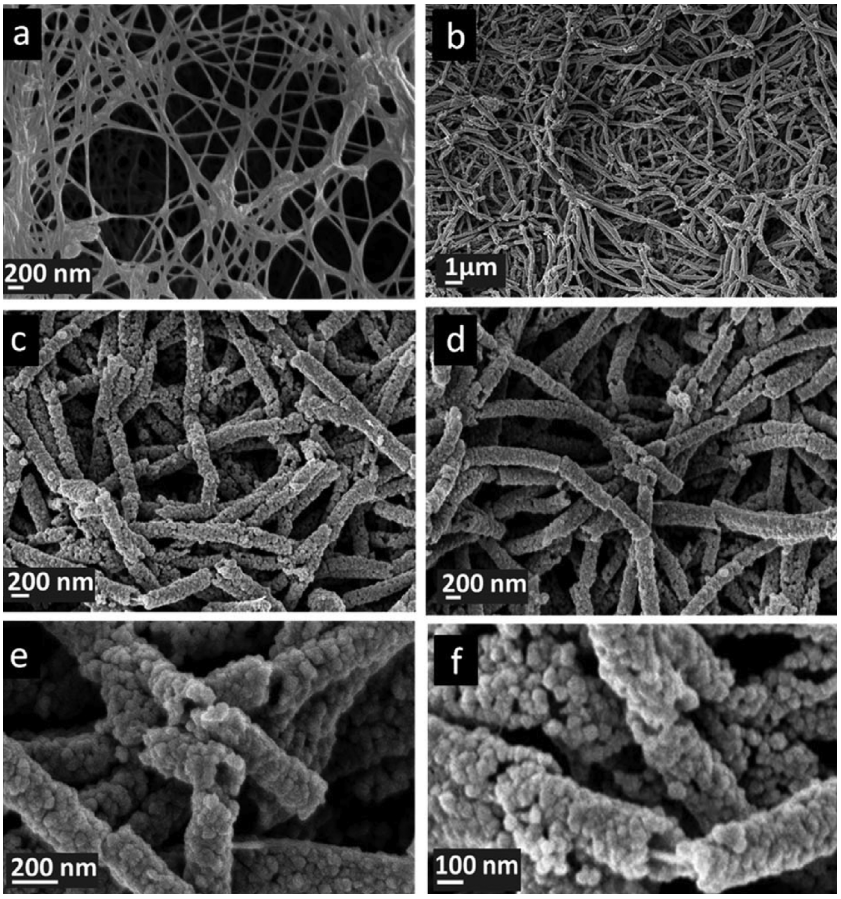

Fig. 1. FE-SEM images of freeze-dried BC (a) and different representative regions of BC-templated-$CoFe_2O_4$ nanotubes (b–f).

3.2. Field emission scanning electron microscopy

The morphology of freeze-dried BC and BC-templated-$CoFe_2O_4$ nanotubes is shown in Fig. 1. Fig. 1a shows a representative scanning electron microscopy image of BC after the freeze-drying process, revealing a tridimensional network consisting of continuous micrometric-in-length nanoribbons and nanoribbons bundles. Although the determination of the width distribution of the nanoribbons is not straightforward due to the frequent twisting of the fibrils and their agglomeration due to extensive hydrogen bonding, manual image analysis of several isolated nanoribbons widths indicated a width interval of 28–83 nm (400 measurements approximately). Moreover, by contrast analysis, the average estimated porosity of the freeze-dried BC was ≈46%.

BC-templated-$CoFe_2O_4$ nanotubes are shown in Fig. 1b–f. In comparison with the BC aerogel shown in Fig. 1a, Fig. 1c and d reveals a much denser network, with an estimated porosity of ≈20%. Fig. 1c–f clearly shows the morphology of the cobalt ferrite nanotubes formed by the proposed protocol, in whose interior BC nanofibrils interconnecting the inorganic hollow nanotubes can be seen (Fig. 1f). Approximately 500 nanotubes diameters were measured using the ImageJ software. Nanotubes showed diameters in the 120–340 nm interval, and an average nanotubes diameter of 217 nm (Fig. 2a).

In reference to the particles that form the nanotubes, Fig. 2b illustrates their diameter distribution. As it is shown $CoFe_2O_4$ nanotubes are formed by agglomerates with diameters ranging from 26 to 102 nm. This phenomenon of agglomeration of $CoFe_2O_4$ nanoparticles was also observed by other researchers when obtaining $CoFe_2O_4$ nanoparticles by coprecipitation without addition of any surfactant that hinders aggregation (Maaz, Mumtaz, Hasanain, & Abdullah, 2007). $CoFe_2O_4$ nanoparticles agglomerates have also been observed in nanotubes (Fu et al., 2012) and nanowires synthesized by other techniques (Camacho Meza, Martínez Pérez, Monreal Romero, & García Casillas, 2009; El-Sheikh, Harraz, & Hessien, 2010; Ersen et al., 2008; Junga et al., 2005).

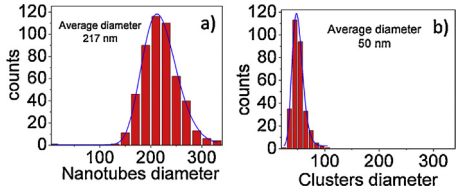

Fig. 2. Diameter distribution of (a) BC-templated-$CoFe_2O_4$ nanotubes and (b) $CoFe_2O_4$ clusters forming the nanotubes.

3.3. X-ray diffraction

The BC-templated-$CoFe_2O_4$ nanotubes structure was analyzed by use of X-ray diffraction (Fig. 3). Qualitative phase identification by XRD allowed determining the corresponding cobalt ferrite reflections with cubic symmetry (JCPDS card No. 22-1086). Only one small peak centred at 22° does not match with the $CoFe_2O_4$ assignment. Although the peak intensity is within the range of measurement error, such reflection could be attributed to the (2 0 0) crystalline plane of bacterial cellulose (Vazquez, Foresti, Cerrutti, & Galvagno, 2013). Cellulose has several crystalline polymorphisms (I, II, III and IV), being cellulose I the crystalline polymorphism naturally produced by bacteria. The intensity of the (2 0 0) peak in cellulose I has the highest intensity of the diffractogram, and it is

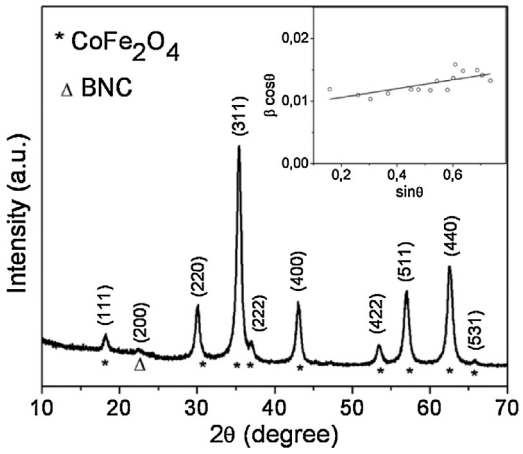

Fig. 3. XRD pattern of BC-templated-$CoFe_2O_4$ nanotubes, inset: Williamson–Hall plot.

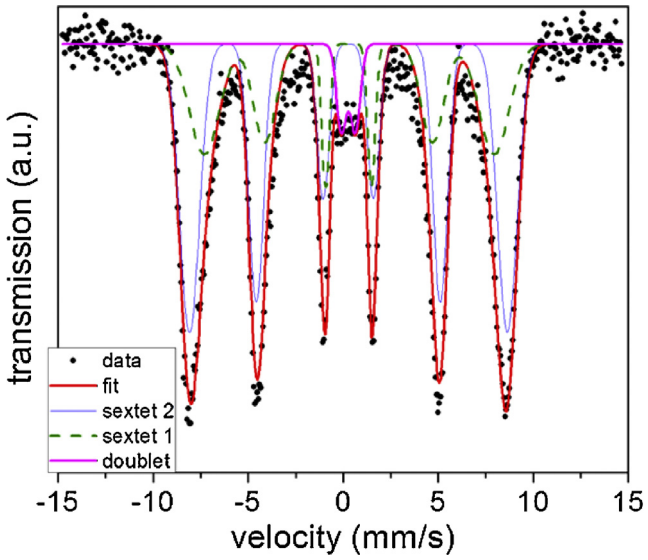

Fig. 4. Mössbauer spectrum of BC-templated-$CoFe_2O_4$ nanotubes.

widely used as representative of the crystalline fraction of cellulose (Park, Baker, Himmel, Parilla, & Johnson, 2010; Segal, Creely, Martin, & Conrad, 1959).

The X-ray pattern indicates some crystal disorder, evidenced by a high background and widened peaks. The high background may be associated with a percentage of amorphous material. Such material may be a combination of bacterial cellulose (its relatively small non-crystalline portion) and cobalt ferrite nanoparticles of very small size.

On the other hand, the observed peak broadening may be due to two main factors, i.e. the effect of crystallite size, and/or the presence of tensions in the network due to microstrains effect. In order to estimate the crystallite size Scherrer (Cullity, 1956) and Williamson–Hall (Hall, 1949; Williamson & Hall, 1953) formulae can be used. Both methods are approximate. In both equations the peak width and position is determined by adjusting the XRD profile with a Lorentzian function. To subtract experimental effects the XRD peaks deconvolution is made by using standard silicon NBS 640 (certificated pattern).

Scherrer equation considers that the particles are spherical and free of tensions in the network. The estimated size should be interpreted as an average dimension perpendicular to the diffraction plane being analyzed. By use of Scherrer approximation the size range of the nanoparticles that form the nanotubes was estimated at 9–13 nm.

The Williamson–Hall method (WH) considers the combined effect of crystallite size and lattice distortion in the diffraction peaks broadening. WH method assumes a small instrumental contribution to broadening when compared with the sample's contribution. The Williamson–Hall approximation can be expressed as (Hall, 1949):

$$\beta \cos\theta = 0.9\lambda/D + 4\varepsilon \sin\theta \quad (1)$$

where, β is the peak width at half height, θ is the position of Bragg diffraction peak, λ is the incident radiation, D is the average crystallite size (nanoparticle) and ε are the microstrains.

To evaluate the contribution of tensions in the network in line broadening, the WH graph was constructed (Fig. 3, inset). This graphic, i.e. $\beta\cos\theta$ vs. $\sin\theta$, is obtained from the information provided by reflections corresponding to the $CoFe_2O_4$ phase. The intercept of the curve with the orderly axis represents the reciprocal of the average crystallite size, and tensions by microstrains can be estimated from the slope of the line. The linear fit of the WH graphic corresponding to $CoFe_2O_4$ indicated an average crystallite size of 15 nm, and a value of 1.7×10^{-3} for microstrains. These values indicate that the contribution of microstrains tensions is low, and that the broadening of the diffraction peaks is mainly determined by the size of the nanoparticles. This result is consistent with the low temperature at which the nanotubes were obtained, which minimizes tension in the network produced by microstrains. Thus, results suggest that crystalline disorder might be primarily associated to the surface effect originated in the small crystallite size, which is actually determined by a limited grain growth due to the low thermal energy involved in the nanotubes synthesis.

3.4. Mössbauer spectroscopy

In order to complement structural analysis of the BC-templated-$CoFe_2O_4$ nanotubes, Mössbauer spectrometry was performed. Room temperature data were fitted with two sextets (magnetic interactions) and a doublet (quadrupole interaction), and an acceptable fitting was obtained (Fig. 4). Sextet 1 corresponds to Fe^{3+} in tetrahedral environment (A-sites), whereas sextet 2 corresponds to Fe^{3+} in octahedral environment (B-sites) of ferrimagnetic cobalt ferrite (Rechenberg & Tourinho, 1991). The spectrum can be described by means of two sextets with mean hyperfine fields of 47.4 and 51.9 T with proportions of 35 and 60.4%, respectively. According to the different isomer shift values for the mentioned sextets (0.28 and 0.33 mm/s respectively), these two components can be ascribed to the presence of Fe^{3+} ions located only in tetrahedral and octahedral sites, respectively, confirming the formation of $CoFe_2O_4$.

Since no impurity phase was detected by XRD, the presence of a quadrupole doublet (with a value of isomer shift of 0.27 mm/s with proportion of 4.6%) may be attributed to a fraction of the $CoFe_2O_4$ nanoparticles in distinct magnetic regime. The hyperfine parameters of the doublet are typical of $CoFe_2O_4$ nanoparticles in superparamagnetic regime, which is characteristic of NPs small size. There are reports of superparamagnetic $CoFe_2O_4$ Nps up of 9 nm (Vandenberghe & Grave, 1989).

The relative intensity of the iron populations was used for calculating the cationic distribution in the spinel. The cation distribution estimated from the subspectra corresponds to the formula $(Co_{0.27}Fe_{0.73})[Co_{0.73}Fe_{1.27}]O_4$ where the round brackets and square brackets denote cation sites of tetrahedral (A) and octahedral (B) coordination, respectively. This indicates that a spinel phase of cobalt ferrite of the reverse type was formed. In agreement with XRD results, Mössbauer spectrometry confirmed the presence of a single inorganic phase.

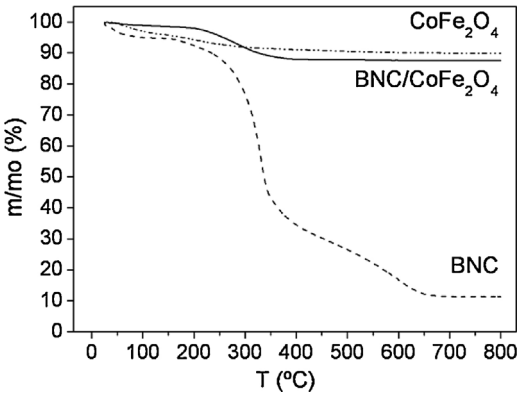

Fig. 5. TG curves of freeze-dried BC, $CoFe_2O_4$ nanoparticles and BC-templated-$CoFe_2O_4$ nanotubes.

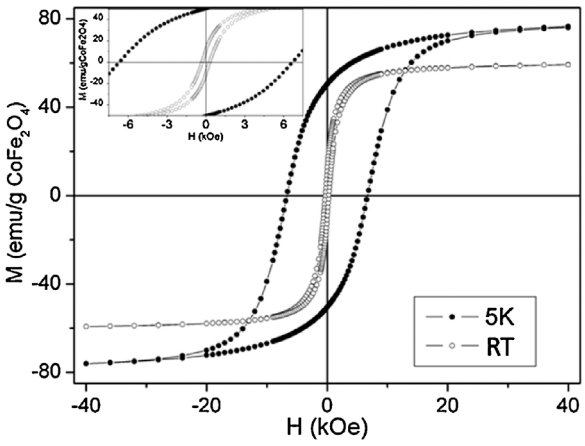

Fig. 6. Magnetization as a function of applied magnetic field at 5 K and room temperature (RT). The inset shows the coercivity for both measurements.

3.5. Thermogravimetric analysis

Thermogravimetric analysis (TGA) was used to examine the thermal stability of the prepared BC-templated-$CoFe_2O_4$ nanotubes, and also to estimate the fraction of BC remaining in their interior. The results are shown in Fig. 5, in comparison with TG data from freeze-dried BC and $CoFe_2O_4$ nanoparticles.

Freeze-dried BC showed three weight losses which resulted in a final residue of 11.4%. The first weight loss (≈5%) occurred from room temperature to 130 °C, and it is associated with the removal of moisture remaining in BC. The second weight loss, characterized by a T_{max} value of 330 °C, is assigned to main cellulose decomposition (Barud, Ribeiro, Capela, Ribeiro, & Messadeq, 2011; Fatyasari et al., 2011). Extending the TG analysis up to 800 °C the presence of a third smaller weight loss between 450 and 600 °C is evidenced, which has been previously attributed to the degradation of polymeric chains and the six-member cyclic structure, pyran (Cheng, Catchmark, & Demirci, 2009).

Within the temperature interval assayed, $CoFe_2O_4$ nanoparticles showed a 10% weight loss. The weight loss observed between room temperature and 150 °C is mainly associated with the evaporation of remaining water (4.5%). The weight loss observed at higher temperatures may be attributed to the elimination of lattice water molecules and dehydroxylation and condensation reactions of remaining metal hydroxides and oxyhydroxides (Yourdkhani & Caruntu, 2011).

The TG curve for BC-templated-$CoFe_2O_4$ nanotubes exhibited an initial 1.3% initial weight loss assigned to remaining moisture, followed by a single decomposition weight loss step with a T_{max} value of 294 °C, assigned to cellulosic template decomposition. The lower T_{max} value for the decomposition of cellulose remaining within the nanotubes may be attributed to the reduced number of effective hydrogen bonds among BC nanoribbons when surrounded by $CoFe_2O_4$ nanotubes. The sample fraction remaining at 800 °C accounted for 87.6%. Under the assumption that in the BC-templated-$CoFe_2O_4$ nanotubes its components decompose in a similar manner than in their individual TG curves, the content of BC remaining within the nanotubes could be estimated in ≈3%.

3.6. Magnetometry measurements

Aiming to determine the magnetic behavior of the obtained nanotubes, magnetization of the sample was recorded as a function of the applied field at room temperature (RT) and at 5 K (Fig. 6). The sample response at room temperature was a hysteresis curve with coercivity (H_c) of 292 Oe and saturation magnetization (M_s) of 59 emu/g (Fig. 6). Whereas the coercivity value is smaller than that for bulk $CoFe_2O_4$ at RT, the saturation magnetization is close to the corresponding one (980 Oe and 65 emu/g, respectively) (Bate, 1980). This can be explained by the presence of a fraction of $CoFe_2O_4$ nanoparticles in superparamagnetic state. The critical size for superparamagnetic relaxation in $CoFe_2O_4$ is within the range of 4–9 nm (Ersen et al., 2008; Kim, Kim, & Lee, 2003). Considering the results from XRD, the nanoparticles average size was near the critical size for a superparamagnetic regime. Moreover, the hysteresis loop at 5 K revealed that both, the coercivity and the magnetization, showed a sizeable increase with respect to the corresponding values at RT (6685 Oe and 76 emu/g, respectively). The values of M_s and Hc of nanotubes at RT, do not differ significantly from those obtained in single nanoparticles (grown without nanocellulose template). Indicating that the matrix does not change the magnetic properties and only acts as a template for the production of a specific structure (Sharifi, Shokrollahi, Doroodmand, & Safi, 2012).

4. Conclusions

In the current contribution, cobalt ferrite nanotubes were successfully synthesized by coprecipitation using bacterial nanocellulose as template. The obtained $CoFe_2O_4$ nanotubes with an average diameter of 217 nm are formed by nanoparticle clusters 26–102 nm in size. The nanoparticles that form the nanotubes have a certain crystalline disorder due to the small crystallite size, and in a lesser extent to the network microstrains. The biotemplated nanotubes have magnetic behavior at room temperature. Magnetic properties are influenced by a fraction of nanoparticles in the superparamagnetic state. The work is currently ongoing in order to get more details about the structural and physical properties of the obtained $CoFe_2O_4$ nanotubes.

Acknowledgements

We thank Dr. Luis Ielpi from "Fundación Instituto Leloir" Buenos Aires, Argentina, for the bacterial strain of *Gluconacetobacter xylinus* (syn. *Acetobacter aceti* subsp. *xylinus*, *Acetobacter xylinum*) NRRL B-42 used in this work.

References

Aoki, Y., Huang, J., & Kunitake, T. (2006). Electro-conductive nanotubular sheet of indium tin oxide as fabricated from the cellulose template. *Journal of Material Chemistry, 16*, 292–297.

Barud, H. S., Ribeiro, C. A., Capela, J. M. V., Ribeiro, S. J. L., & Messadeq, Y. (2011). Kinetic parameters for thermal decomposition of microcrystalline, vegetal, and bacterial cellulose. *Journal of Thermal Analysis and Calorimetry, 105*, 421–426.

Bate, G. (1980). *Ferromagnetic Materials*. North-Holland: Amsterdam.

Bielecki, S., Krystynowicz, A., Turkiewicz, M., & Kalinowska, H. (2002). Biopolymers. In S. D. B. E. J. Vandamme, & A. Steinbüchel (Eds.), *Polysaccharides I* (5) (pp. 37–90). Germany: Wiley-Blackwell.

Camacho Meza, J. G., Martínez Pérez, C. A., Monreal Romero, H., & García Casillas, P. E. (2009). Synthesis of Cobalt Ferrite Nanowires Using FeOOH as a Template. *Solid State Phenomena*, *151*, 245–251.

Castro, C., Zuluaga, R., Putaux, J.-L., Caroa, G., Mondragon, I., & Gañan, P. (2011). Structural characterization of bacterial cellulose produced by *Gluconacetobacter swingsii* sp. from Colombian agroindustrial wastes. *Carbohydrate Polymers*, *84*, 96–102.

Cullity, B. D. (1956). *Elements Of X-ray Diffraction*. Massachusetts: Addison-Wesley Publishing Company.

Charreau, H., Foresti, M. L., & Vázquez, A. (2013). Nanocellulose patents trends: a comprehensive review on patents on cellulose nanocrystals, microfibrillated and bacterial cellulose. *Recent Patents on Nanotechnology*, *7*, 56–80.

Chen, J., Yang, P., Ma, Y., & Wu, T. (2011). Characterization of chitosan magnetic nanoparticles for in situ delivery of tissue plasminogen activator. *Carbohydrate Polymers*, *84*, 364–372.

Cheng, K.-C., Catchmark, J. M., & Demirci, A. (2009). Effect of different additives on bacterial cellulose production by *Acetobacter xylinum* and analysis of material property. *Cellulose*, *16*, 1033–1045.

Dorsey, P. C., Lubitz, P., Chrisey, K. B., & Horwitz, J. S. (1996). Phase formation and crystallinity-dependent magnetic parameters of $Co_{1-x}Fe_{2+x}O_4$ nanoparticals. *Journal of Applied Physics*, *79*, 6338.

El-Sheikh, S. M., Harraz, F. A., & Hessien, M. M. (2010). Magnetic behavior of cobalt ferrite nanowires prepared by template-assisted technique. *Materials Chemistry and Physics*, *123*, 254–259.

Ersen, O., Bégin, S., Houllé, M., Amadou, J., Janowska, I., Grenèche, J., et al. (2008). Microstructural investigation of magnetic $CoFe_2O_4$ nanowires inside carbon nanotubes by electron tomography. *Nano Letters*, *8*, 1033–1040.

Fatyasari, I., Sureshkumar, M., & Lee, C.-K. (2011). One-pot preparation of amine-rich magnetite/bacterial cellulose nanocomposite and its application for arsenate removal. *RSC Advances*, *1*, 625–631.

Fu, J., Zhang, J., Peng, Y., Zhao, J., Tan, G., Mellors, N. J., et al. (2012). Unique magnetic properties and magnetization reversal process of $CoFe_2O_4$ nanotubes fabricated by electrospinning. *Nanoscale*, *4*, 3932–3936.

Gu, Y., Liu, X., Niu, T., & Huang, J. (2010). Superparamagnetic hierarchical material fabricated by protein molecule assembly on natural cellulose nanofibres. *Chemical Communications*, *46*, 6096–6098.

Hall, W. H. (1949). X-ray line broadening in metals. *Proceedings of the Physical Society of London*, *A62*, 741–743.

Hassan-Nejad, M., Ganster, J., Bohn, A., Pinnow, M., & Volkert, B. (2009). Bio-based nanocomposites of cellulose acetate and nano-clay with superior mechanical properties. *Macromolecular Symposia*, *280*, 123–129.

Hu, W., Chen, S., Yang, J., Li, Z., & Wang, H. (2014). Functionalized bacterial cellulose derivatives and nanocomposites. *Carbohydrate Polymers*, *101*, 1043–1060.

Hua, Z. H., Chen, R. S., Li, C. L., Yang, S. G., Lu, M., Gu, B. X., et al. (2007). $CoFe_2O_4$ nanowire arrays prepared by template-electrodeposition method and further oxidization. *Journal of Alloys and Compounds*, *427*, 199–203.

Junga, J.-S., Lim, J.-H., Choi, K.-H., Oh, S.-L., Smith, Y. D. A., Stokes, K. L., et al. (2005). $CoFe_2O_4$ nanostructures with high coercivity. *Journal of Applied Physics*, *97*(10), F306.

Kim, Y. I., Kim, D., & Lee, C. S. (2003). Synthesis and characterization of $CoFe_2O_4$ magnetic nanoparticles prepared by temperature-controlled coprecipitation method. *Physica B*, *337*, 42–51.

Klemm, D., Kramer, F., Moritz, S., Lindström, T., Ankerfors, M., & Gray, D. (2011). Nanocelluloses: A new family of nature-based materials. *Angewandte Chemie International Edition*, *50*(24), 5438–5466.

Klemm, D., Shumman, D., Kramer, F., Hessler, N., Hornung, M., & Schmauder, H.-P., et al. (Eds.). (2006). *Polysaccharides II*. Berlin, Heilderberg: Springer.

Korhonen, J. T., Hiekkataipale, P., Malm, J., Karppinen, M., Ikkala, O., & Ras, R. H. A. (2011). Inorganic hollow nanotube aerogels by atomic layer deposition onto native nanocellulose templates. *ACS Nano*, *5*(3), 1967–1974.

Kroll, E., & Winnik, F. M. (1996). In situ preparation of nanocrystalline g-Fe_2O_3 in iron(II) cross-linked alginate gels. *Chemistry of Materials*, *8*, 1594–1596.

Li, F., Yao, X., Wang, Z., Xing, W., Jin, W., Huang, J., et al. (2012). Highly porous metal oxide networks of interconnected nanotubes by atomic layer deposition. *Nano Letters*, *12*, 5033–5038.

Llanes, F., Ryan, D. H., & Marchessault, R. H. (2000). Magnetic nanostructured composites using alginates of different M/G ratios as polymeric matrix. *International Journal of Biological Macromolecules*, *27*, 35–40.

Maaz, K., Mumtaz, A., Hasanain, S. K., & Abdullah, C. (2007). Synthesis and magnetic properties of cobalt ferrite ($CoFe_2O_4$) nanoparticles prepared by wet chemical route. *Journal of Magnetism and Magnetic Materials*, *308*, 289–295.

Olsson, R. T., Salazar-Alvarez, G., Hedenqvist, M. S., Gedde, U. W., Lindberg, F., & Savage, S. J. (2005). Controlled synthesis of near-stoichiometric cobalt ferrite nanoparticles. *Chemistry of Materials*, *17*, 5109–5118.

Olsson, R. T., Samir, M. A. S. A., Salazar-Alvarez, G., Belova, L., Ström, V., Berglund, L. A., et al. (2010). Making flexible magnetic aerogels and stiff magnetic nanopaper using cellulose nanofibrils as templates. *Nature Nanotechnology*, *5*, 584–588.

Park, S., Baker, J. O., Himmel, M. E., Parilla, P. A., & Johnson, D. (2010). Cellulose crystallinity index: Measurement techniques and their impact on interpreting cellulase performance. *Biotechnology for Biofuels*, *3*, 1–10.

Putra, A., Kakugo, A., Furukawa, H., Gong, J. P., & Osada, Y. (2008). Tubular bacterial cellulose gel with oriented fibrils on the curved surface. *Polymer*, *49*, 1885–1891.

Rechenberg, H. R., & Tourinho, F. A. (1991). Mossbauer spectroscopic characterization of manganese and cobalt ferrite ferrofluids. *Hyperfine Interactions*, *67*, 627–632.

Schneider, C. A., Rasband, W. S., & Eliceiri, K. W. (2012). NIH image to imagej: 25 year of image analysis. *Nature Methods*, *9*, 671–675.

Segal, L., Creely, J. J., Martin, A. E., & Conrad, C. M. (1959). An empirical method for estimating the degree of crystallinity of native cellulose using the X-ray diffractometer. *Textile Research Journal*, *29*, 786–794.

Sharifi, I., Shokrollahi, H., Doroodmand, M., & Safi, R. (2012). Magnetic and structural studies on $CoFe_2O_4$ nanoparticles synthesized by co-precipitation, normal micelles and reverse micelles methods. *Journal of Magnetism and Magnetic Materials*, *324*, 1854–1861.

Shilin, L., Qiufang, Y., Dandan, T., Tengfei, Y., & Xiaoya, L. (2012). Highly flexible magnetic composite aerogels prepared by using cellulose nanofibril networks as templates. *Carbohydrate Polymers*, *89*, 551–557.

Tourinho, F. A., Franck, R., & Massart, R. (1990). Aqueous ferrofluids based on manganese and cobalt ferrites. *Journal of Materials Science*, *25*, 3249–3254.

Valenzuela, R. (1994). *Magnetic ceramics*. Cambridge, UK: Cambridge University Press.

Vandenberghe, R. E., & Grave, E. D. (1989). Mossbauer effect studies of oxidic spinels. In F. Granjdjean, & G. J. Long (Eds.), *Mossbauer Spectroscopy Applied to Inorganic Chemistry* (pp. 59–182). New York: Plenum Press. Chapter 3.

Vazquez, A., Foresti, M. L., Cerrutti, P., & Galvagno, M. (2013). Bacterial cellulose from simple and low cost production media by *Gluconacetobacter xylinus*. *Journal of Polymers and the Environment*, *21*(2), 545–554.

Williamson, K., & Hall, W. H. (1953). X-ray line broadening from filed aluminium and wolfram. *Acta Metallurgica et Materialia*, *1*, 22–31.

Yourdkhani, A., & Caruntu, G. (2011). Highly ordered transition metal ferrite nanotube arrays synthesized by template-assisted liquid phase deposition. *Journal of Materials Chemistry*, *21*, 7145–7153.

Zhang, W., Chen, S., Hu, W., Zhou, B., Yang, Z., Yin, N., et al. (2011). Facile fabrication of flexible magnetic nanohybrid membrane with amphiphobic surface based on bacterial cellulose. *Carbohydrate Polymers*, *86*, 1760–1767.

Zheng, G., Cui, Y., Karabulut, E., Wågberg, L., Zhu, H., & Hu, L. (2013). Nanostructured paper for flexible energy and electronic devices. *MRS Bulletin*, *38*, 320–325.

Zhoua, Y., Branford-White, C., Nie, H., & Zhua, L. (2009). Adsorption mechanism of Cu^{2+} from aqueous solution by chitosan-coated magnetic nanoparticles modified with a-ketoglutaric acid. *Colloids and Surfaces B*, *74*, 244–252.